Interdecadal Pacific Oscillation responsible for the linkage of decadal changes in precipitation/moisture in arid central Asia and humid Asian monsoon region during the last millennium

Hongna Xu[1], Tao Wang[1,2,*], Huijun Wang[1,2]

[1] Collaborative Innovation Center on Forecast and Evaluation of Meteorological Disasters (CIC-FEMD), Nanjing University of Information Science and Technology, Nanjing 210044, China

[2] Climate Change Research Center and Nansen-Zhu International Research Centre, Institute of Atmospheric Physics, Chinese Academy of Sciences, Beijing 100029, China

* Corresponding author: Tao Wang (wangtao@mail.iap.ac.cn)

14 **Abstract**

15 Reconstruction and observational studies imply a potential linkage of

16 moisture/precipitation change in arid central Asia and monsoonal East Asia, in which

17 the evolution of moisture/precipitation in central Asia is out-of-phase with that in

18 northern China, but in-phase with that in southern China. In order to ascertain whether

19 there is a robust linkage between the changes in climate in Asian arid regions and

20 monsoon regions and to elucidate the underlying dynamic mechanisms, we analyzed

21 the Last Millennium Reanalysis dataset and outputs from the Community Earth

22 System Model-Last Millennium Ensemble (CESM-LME). The results indicate a

23 significant decadal linkage between precipitation changes in central Asia's arid region

24 and the Asian monsoon region during the last millennium, which is primarily driven

25 by the Interdecadal Pacific Oscillation (IPO). In spring, the positive IPO could

26 enhance westerlies over the Mediterranean Sea and to its east, which could transport

27 more water vapor and cause increased precipitation over central Asia. In summer, the

28 positive IPO is accompanied with weakened Asian monsoon and southward Asian

29 subtropical westerly jet, which can lead to increased (decreased) summer precipitation

30 over southern China (over northern China and South Asia). The IPO plays a dominant

31 role in connecting the decadal variations in precipitation between arid central Asia and

32 monsoonal Asia by modulating the precipitation of their respective major rainy

33 seasons. Model results suggest that this decadal linkage stems entirely from the

34 internal variability present in the CESM-LME control and all single-forcing

35 simulations. Changes in external forcing factors do not alter this inherent linkage

36   caused by IPO. Moreover, based on analyses of the aridity index and soil moisture

37   content, this relationship of precipitation variation also causes a similar decadal

38   linkage of moisture changes in central Asia and monsoonal Asia. The differences in

39   the multi-centennial-scale moisture/precipitation variations in the Asian arid region

40   and the monsoon region between the Medieval Climate Anomaly and Little Ice Age

41   are also likely caused by IPO-like sea surface temperature anomalies.

1 Introduction

The climate of the mid- to low-latitude Asian continent is characterized by an arid central Asian region and a moist monsoonal region. The climate in central Asia is mainly controlled by westerlies as a result of its geographical location and blocking by plateaus and mountains to the southeast (Chen et al., 2010). The main rainy seasons are spring and winter, especially in southern central Asia (Aizen et al., 2001; Chen et al., 2011; Xu et al., 2020; Wang et al., 2022). By contrast, the climate in monsoonal Asia is mainly controlled by the East Asian monsoon and the South Asian monsoon. The main rainy season is summer as a result of the warm, moist East Asian summer monsoon (Ding and Chan, 2005) and the South Asian summer monsoon (Turner and Annamalai, 2012).

The Asian arid and monsoonal climates should be independent of each other due to the dominance of different systems. However, the reconstruction records suggest a strong linkage between them on a centennial scale. Chen et al. (2015) reviewed numerous reconstruction studies and indicated that the climate was relatively wetter in central Asia and southern China, whereas it was relatively drier in northern China during the Little Ice Age (LIA; 1400–1900 AD) (Fig. 1). During the earlier Medieval Climate Anomaly (MCA; 1000–1300 AD), the wet and dry changes were the opposite, with drier conditions in central Asia and southern China and wetter conditions in northern China.
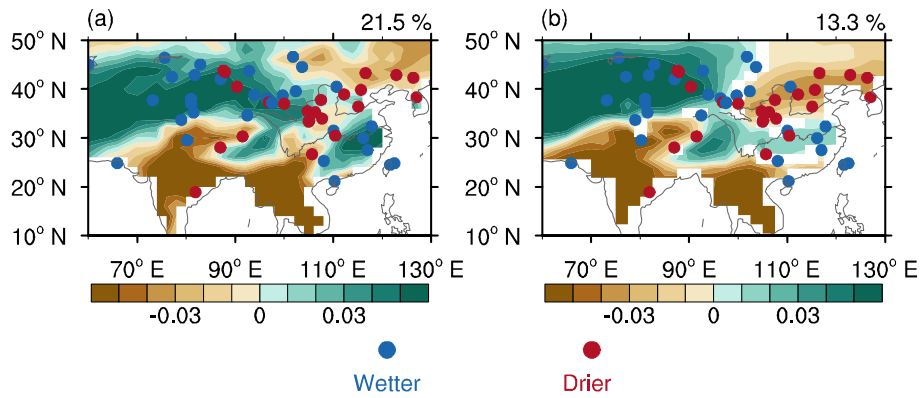
Figure 1. The reconstructed and simulated first leading precipitation mode. **(a)** The first leading mode (EOF1) of the nine-year low-pass Lanczos filtered annual precipitation for the time period 850–2000 in the Last Millennium Reanalysis (LMR) dataset. The explained variance is given at the top-right. **(b)** The average EOF1 of the nine-year low-pass Lanczos filtered annual precipitation in CESM-LME 12 all-forcing simulations for the time period 850–2005; the shading shows where at least two-thirds of the members agree on the sign of the average value. The averaged explained variance is given at the top-right. The dots represent the reconstructed precipitation/moisture records modified from Chen et al. (2015); the blue (red) dots denote wetter (drier) conditions in the LIA than in the MCA.

Clues to the linkage between the climate of the Asian arid regions and the Asian monsoon regions can also be found based on the limited length of observational data from the modern era. Since the mid-20th century, the central Asia has become wetter (Shi et al., 2007; Jiang et al., 2009; Chen et al., 2011; Huang et al., 2013). During the same period, southern China experienced more precipitation, whereas northern China received less precipitation and became drier (Ding et al., 2008; Zhao et al., 2010; Wang et al., 2013). Focusing on two different climatic regions, the precipitation observations during the period of 1960-2010 also show similar linkage (Huang et al., 2015). On a decadal scale, central Asia experienced more (less) summer precipitation, southern China received more (less) summer precipitation, whereas northern China

83   received less (more) summer precipitation.

84   However, the reconstruction records of the last millennium and the 50-year

85   observational data only cover less than two periods on the multi-centennial or

86   interdecadal scale, respectively. It is not sufficient to demonstrate a significant

87   relationship between the climate of the Asian arid regions and the Asian monsoon

88   regions. The specific mechanisms behind this possible linkage are still not clear. In

89   addition, modeling results also indicate that only one out of nine coupled models

90   within the Paleoclimate Modeling Intercomparison Project Phase 3 (PMIP3) is able to

91   reproduce the similar climatic linkage between the Asian arid and monsoonal regions

92   during the MCA and LIA (Shi et al., 2016). Due to the limitations of data length on

93   the time scales of interest and the large uncertainty in existing model results, therefore,

94   further research is still needed to confirm whether there is an inherent connection

95   between the arid regions and monsoon regions in Asia in terms of their dry-wet

96   variations.

97   In this study, we first focus on the decadal scale and intend to analyze whether

98   there is a robust linkage between the changes in precipitation pattern in arid regions

99   and monsoon regions in Asia using the newly released Last Millennium Reanalysis

100   (LMR) dataset (Tardif et al., 2019; Anderson et al., 2019). Additionally, to further

101   explore the possible mechanisms underlying the linkage and the potential impacts of

102   different external forcing factors, the Community Earth System Model Last

103   Millennium Ensemble (CESM-LME, Otto-Bliesner et al., 2016) is also utilized

104   because of its good performance in simulating Asian precipitation and summer

monsoon (e.g., Hu et al., 2023; Mishra and Aadhar, 2021; Shi et al., 2018) and the

availability of multiple samples forced by different forcing factors. Thus, the aim of

this study is to investigate the linkage between precipitation/moisture changes in arid

central Asia and monsoonal Asia during the last millennium and its driving factors.

The data and methods used in this study are described in detail in Sect. 2. The linkage

between the changes in precipitation/moisture pattern in arid regions and monsoon

regions in Asia is examined and its driving factors are analyzed in Sect. 3. Finally, the

discussion and conclusions are presented in Sect. 4 and Sect. 5, respectively.

2 Data and methods

2.1 Reanalysis data and simulations

In this study, we used the reconstructed annual precipitation anomalies (relative

to the climatological mean of 1951–1980) at a spatial resolution of 2° for the time

period 850–2000 from the LMR Version 2.1 dataset (Tardif et al., 2019; Anderson et

al., 2019) to examine the possible linkage between the Asian arid and monsoonal

regions. The proxy records assimilated in the LMR Version 2.1 dataset are from

PAGES-2k (PAGES2k, 2017). The analyses based on LMR were started with the

"grand mean", which was an average of 20 LMR reconstructions contained in

aforementioned array. In addition, the reconstructed sea surface temperature (SST)

anomalies from the LMR Version 2.1 dataset are also used to verify the model results.

In order to investigate the underlying mechanisms, we analyzed the monthly

outputs of CESM-LME project (Otto-Bliesner et al., 2016). The CESM-LME

simulations are performed using the CESM 1.1 model, in which the atmospheric

127   component is the Community Atmosphere Model Version 5 (CAM5) (Hurrell et al.,

128   2013). The atmosphere and land (ocean and sea ice) components in the CESM-LME

129   simulations have the same ~2° (~1°) horizontal resolutions as the CESM1.1 model.

130   We analyzed a total of 35 CESM-LME simulations: one control simulation, 12

131   all-forcing simulations and 22 single-forcing simulations. The single-forcing

132   simulations included a subset of five simulations forced by volcanic eruptions, a

133   subset of four simulations forced by solar activity, a subset of four simulations forced

134   by ozone and aerosols, three subsets of three simulations forced by greenhouse gases,

135   land use and land cover, and the Earth's orbit, respectively. The subset of simulations

136   forced by ozone and aerosols covered the time period 1850–2005, whereas the other

137   simulations were available for the time period 850–2005. The analyses for the

138   all-forcing simulations and the six subsets of single-forcing simulations were all based

139   on the arithmetic mean of multiple members, which was the final step in the analyses.

140   In addition, we also referred to reconstructed moisture/precipitation changes

141   (relative to the median of entire last millennium) in the LIA and MCA summarized by

142   Chen et al. (2015). The reconstructions synthesized by Chen et al. (2015) include 71

143   moisture/precipitation records derived from different types of proxy records (i.e., lake

144   record, speleothem record, historical documents, tree-ring record, ice-core record,

145   marine record, peat record, aeolian record, and river terrace). Based on these

146   moisture/precipitation records, figure 3 in Chen et al. (2015) provided the wetness

147   grades (i.e., the wetness was classified into dry, moderately dry, moderate, moderately

148   wet, and wet) for the LIA and MCA at individual sites. The 55 moisture/precipitation

149 records with different wetness grades between the LIA and MCA were selected in this

150 study to explore the moisture/precipitation changes between these two periods.

151 **2.2 Methods**

152 Following Henley et al. (2015), we defined the Interdecadal Pacific Oscillation

153 (IPO) index as the difference between the SST anomalies averaged over the

154 central-eastern equatorial Pacific (10 °S–10 °N, 170 °E–90 °W) and the average of the

155 SST anomalies over the western-central subtropical North Pacific (25–45 °N, 140 °E–

156 145 °W) and the western-central subtropical South Pacific (50–15 °S, 150 °E–160 °

157 W). The base period for calculating the IPO index was 1850–1900. To obtain the

158 filtered version of the index, a nine-year low-pass Lanczos filter was used, coinciding

159 with the other analyses in this study.

160 We used the aridity index (AI) to quantify the moisture condition of the

161 terrestrial climate (Middleton and Thomas, 1997):

162 $$AI = \frac{P}{PET} \tag{1}$$

163 where P is the annual precipitation (units: mm day^{-1}), representing the water supply to

164 land and PET is the annual potential evapotranspiration (units: mm day^{-1}), which

165 measures the atmospheric demand of water. A larger aridity index indicates that

166 relatively more moisture remains in the land, whereas a smaller aridity index

167 represents drier condition. The outputs of the CESM-LME simulations for soil

168 moisture (top 10 cm of soil; units: kg m^{-2}) were also analyzed to examine the analyses

169 based on the aridity index. Thus, the analyses related to moisture conditions in this

170 study were based on both the aridity index and soil moisture content.

171   The Penman–Monteith algorithm (Penman, 1948; Monteith, 1965) is widely

172   used to estimate the potential evapotranspiration and is recommended as a standard

173   method by the Food and Agriculture Organization of the United Nations (Allen et al.,

174   1998):

175    $$PET = \frac{0.408\Delta(R_\mathrm{n}-G)+\gamma\frac{900}{T_\mathrm{mean}+273}U(e_\mathrm{s}-e_\mathrm{a})}{\Delta+\gamma(1+0.34U)} \tag{2}$$

176   where the R_n is the net surface radiation (units: MJ m^{-2} day^{-1}), the G is soil heat flux

177   density (units: MJ m^{-2} day^{-1}); the difference between them represents the available

178   energy. γ is the psychrometric constant (units: kPa °C^{-1}), T_mean is the mean

179   temperature (units: °C; i.e., the average of the 2-m daily maximum and daily

180   minimum air temperatures); Δ is the slope vapor pressure curve (units: kPa °C^{-1})

181   derived from T_mean, U is the 2-m wind speed (units: m s^{-1}); e_s is the saturation vapor

182   pressure (units: kPa), derived from the daily maximum and daily minimum air

183   temperatures; e_a is the actual vapor pressure (units: kPa), calculated from e_s and the

184   relative humidity.

185   Empirical orthogonal function (EOF) analysis was performed on the

186   standardized annual precipitation to identify the first leading precipitation mode over

187   the Asian continent. A nine-year low-pass Lanczos filter was applied to the

188   standardized precipitation before EOF analysis to remove the variability on

189   interannual and shorter timescales. The same analyses were also applied to the aridity

190   index and the annual soil moisture content to obtain the first leading decadal moisture

191   mode over the Asian continent. Linear regression and correlation analyses were

192   applied to understand the root cause of the leading decadal precipitation/moisture

193   modes and their statistical significance was examined by a two-sided t-test. Because

194   of the low-pass Lanczos filter before linear regression and correlation analyses, the

195   effective degree of freedom N^* in the t-test was calculated following Bretherton et al.

196   (1999):

197    $$N^* = N \frac{1-r_a r_b}{1+r_a r_b} \qquad (3)$$

198   where r_a (r_b) is the autocorrelation at lag 1 for variables a (b) and N is the original

199   length of the time series. A two-sided t-test was also applied to examine the statistical

200   significance of climate changes between the LIA and the MCA. Besides, the

201   consistency of results derived from multiple members (i.e., analyses based on

202   all-forcing simulations and the six subsets of single-forcing simulations) was

203   examined by counting the percentage of members whose results' signs are the same as

204   the arithmetic mean of multiple members. A power spectrum analysis was performed

205   on the time series of the leading precipitation mode and the IPO index to obtain their

206   dominant periodicity, the statistical significance of which was examined via the power

207   spectrum of the mean red noise (Gilman et al., 1963).

208   In this study, winter, spring, summer, and autumn were defined as December–

209   February, March–May, June–August, and September–November, respectively.

210   **3 Results**

211   **3.1 Reconstructed and simulated first leading precipitation mode**

212   Based on the LMR data, the first leading mode (EOF1) of the decadal changes in

213   Asian precipitation in the last millennium showed the same changes in precipitation in

214   arid central Asia and southern China, which were the opposite of those in the South

215   Asian monsoon region (including the southern Tibetan Plateau, the Indian Peninsula

216   and the Indo-China Peninsula) and most of northern China (Fig. 1a). This mode

217   accounted for 21.5% of the total variance of precipitation in Asia in the last

218   millennium.

219   We also analyzed the outputs of the CESM-LME simulations. In the all-forcing

220   simulations, most members reproduced similar first leading precipitation mode with

221   the reconstruction for the time period 850–2005 (Fig. S1). Their ensemble pattern was

222   also consistent with the reconstruction (Fig. 1b). The averaged explained variance was

223   13.3% (ranging from 11.7 to 14.8%). These same patterns of changes in precipitation

224   between the long-term simulations and the reconstruction suggest that, on the decadal

225   scale, there is a robust linkage between the changes in precipitation pattern in arid

226   regions and monsoon regions. This decadal linkage suggests that the evolution of

227   precipitation in central Asia is out-of-phase with that in northern China and South

228   Asian monsoon region, but in-phase with that in southern China. The linkage between

229   the arid central Asian region and the East Asian monsoon region is consistent with the

230   relationship of changes in precipitation based on observational data for the last 60

231   years (Huang et al., 2015). Our analysis suggests that this observed relationship has

232   persisted over the last millennium. Our results also indicated that the decadal changes

233   in precipitation in the South Asian monsoon region are also closely related to the

234   changes in the arid central Asian region and the East Asian monsoon region.

235   **3.2 Dominant role of the IPO**

236   Many studies have shown that the SST anomaly is an important factor in

modulating the decadal variability in precipitation over Asia (e.g., Chu et al., 2018;

Huang et al., 2019). We therefore calculated the linear regression of the SST onto the

time series of the leading precipitation mode. Figure 2a and 2c show that higher

(lower) SSTs appeared over the central-eastern equatorial Pacific (the western-central

parts of both the subtropical North Pacific and South Pacific) in the LMR and

all-forcing simulations. The Pacific basin-wide SST anomalies resembled the positive

pattern of the IPO (Power et al., 1999; Henley et al., 2015; Wang and Miao, 2018).

The precipitation anomalies during the positive phases of the IPO showed positive

anomalies in arid central Asia and southern China and negative anomalies in the

South Asian monsoon region and most of northern China (Fig. 2b and 2d), resembling

the leading decadal precipitation mode in the LMR and all-forcing simulations. It is

therefore likely that the IPO dominated the decadal linkage between the changes in

precipitation pattern in arid regions and monsoon regions in Asia.
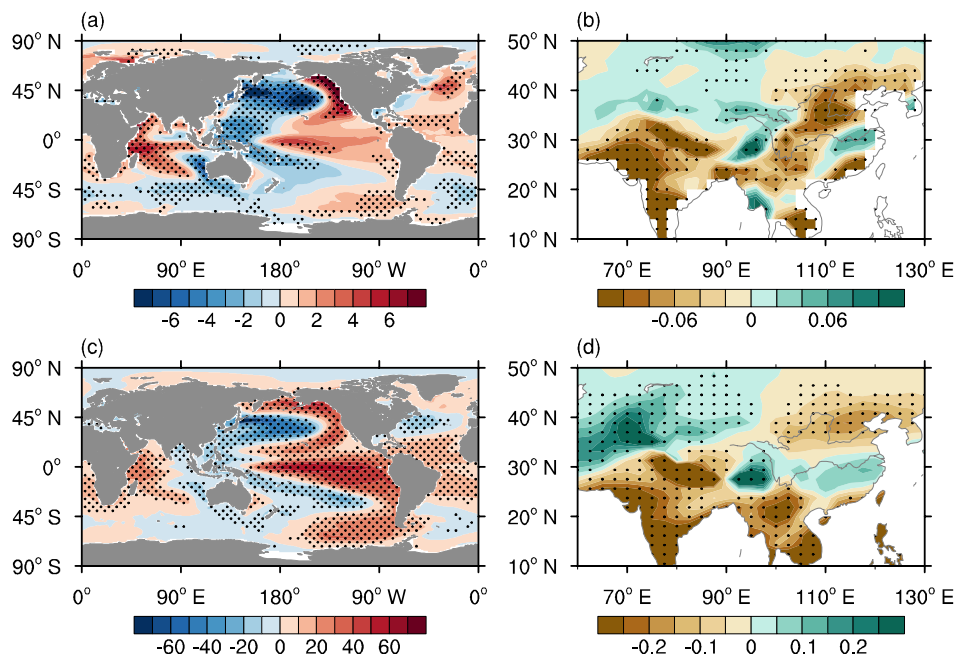
Figure 2. The dominant role of the IPO. The reconstructed **(a)** annual SST anomalies (units: °C)

regressed onto the time series of the leading decadal precipitation mode and **(b)** annual

253 precipitation anomalies (units: mm day^{-1}) regressed onto the time series of the IPO index in the

254 LMR dataset. The dots in parts (**a**, **b**) show significant anomalies at the 95% confidence level. (**c**)

255 Annual SST anomalies (units: °C) regressed onto time series of the leading decadal precipitation

256 mode and (**d**) annual precipitation anomalies (units: mm day^{-1}) regressed onto the time series of

257 the IPO index simulated by multiple members of the CESM-LME all-forcing runs. Dots in parts (**c**,

258 **d**) show that at least two-thirds of the members simulate significant changes (at the 95%

259 significance level), and these significant changes agree on the sign of the average of multiple

260 members.

261   We applied power spectrum analysis to explore the temporal characteristics of

262 the first leading precipitation mode and the IPO. Both the leading precipitation mode

263 and the IPO had a common frequency band of 10–20 years in the LMR and

264 all-forcing simulations (Figs. S2–4), indicating that the IPO dominated the linkage

265 between the changes in precipitation pattern in arid regions and monsoon regions in

266 Asia at decadal to bi-decadal scales during the last millennium. The consistency

267 between the reconstruction and the simulations indicates the reliability of the

268 simulations, which is the foundation of the following analyses on the relevant

269 mechanism based on simulations.

270 **3.3 Processes of the IPO modulating the leading precipitation pattern**

271   Because there is a seasonal cycle in precipitation and the atmospheric circulation

272 over Asia, especially over monsoonal Asia, we analyzed the seasonal changes in

273 precipitation associated with the IPO. During the positive phases of IPO, in the arid

274 central Asia, the precipitation in the four seasons all increased and made a positive

275 contribution to the increase in annual precipitation (Fig. 3). The precipitation

276 anomalies were larger in spring and winter, especially in spring, in which season the

277 precipitation accounted for the most of the annual precipitation (Fig. S5). The largest

278 increase in spring precipitation was mainly in southern central Asia. In East Asia,

279 summer precipitation increased (decreased) over southern (northern) China and

280 autumn precipitation decreased over northern China, both contributing positively to

281 the annual changes in precipitation. By contrast, spring and winter precipitation both

282 decreased over southern China, partly offsetting the positive contribution of summer

283 precipitation to the increase in annual precipitation in this region. Precipitation in all

284 four seasons decreased in most of the South Asian monsoon regions, contributing

285 positively to the decrease in annual precipitation. Then, we analyzed the seasonal

286 atmospheric circulation anomalies associated with the IPO to determine the processes

287 by which the IPO modulated these seasonal changes in precipitation.
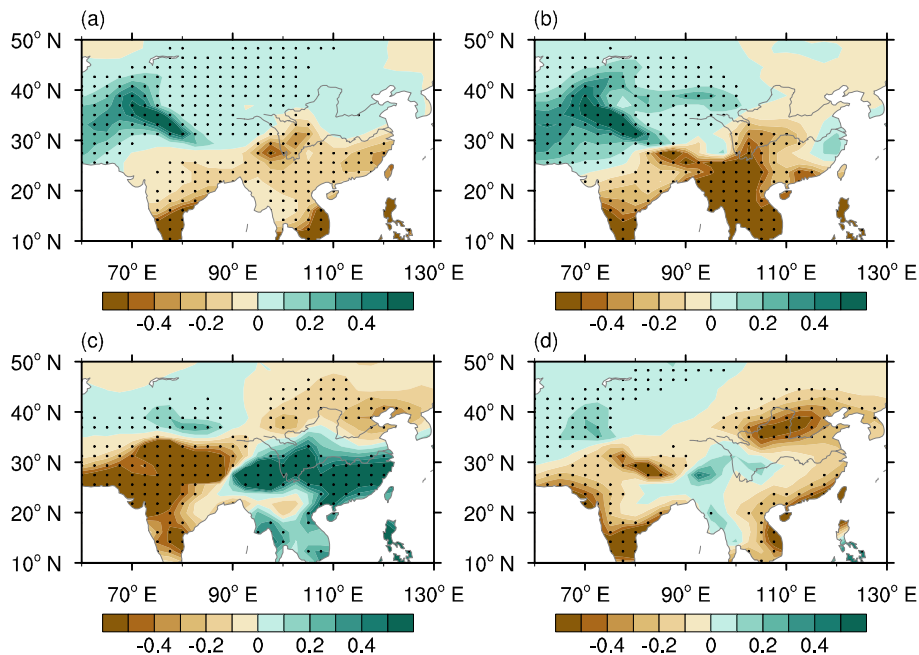
288

289 **Figure 3.** Simulated seasonal precipitation anomalies during the positive phases of the IPO.

290 Regressed maps of **(a)** winter, **(b)** spring, **(c)** summer, and **(d)** autumn precipitation anomalies

291 (units: mm day^{-1}) onto the time series of the IPO index simulated by multiple members of the

292 CESM-LME all-forcing runs. Dots show that at least two-thirds of the members simulate

293 significant changes (at the 95% significance level), and these significant changes agree on the sign

294 of the average of multiple members.

295
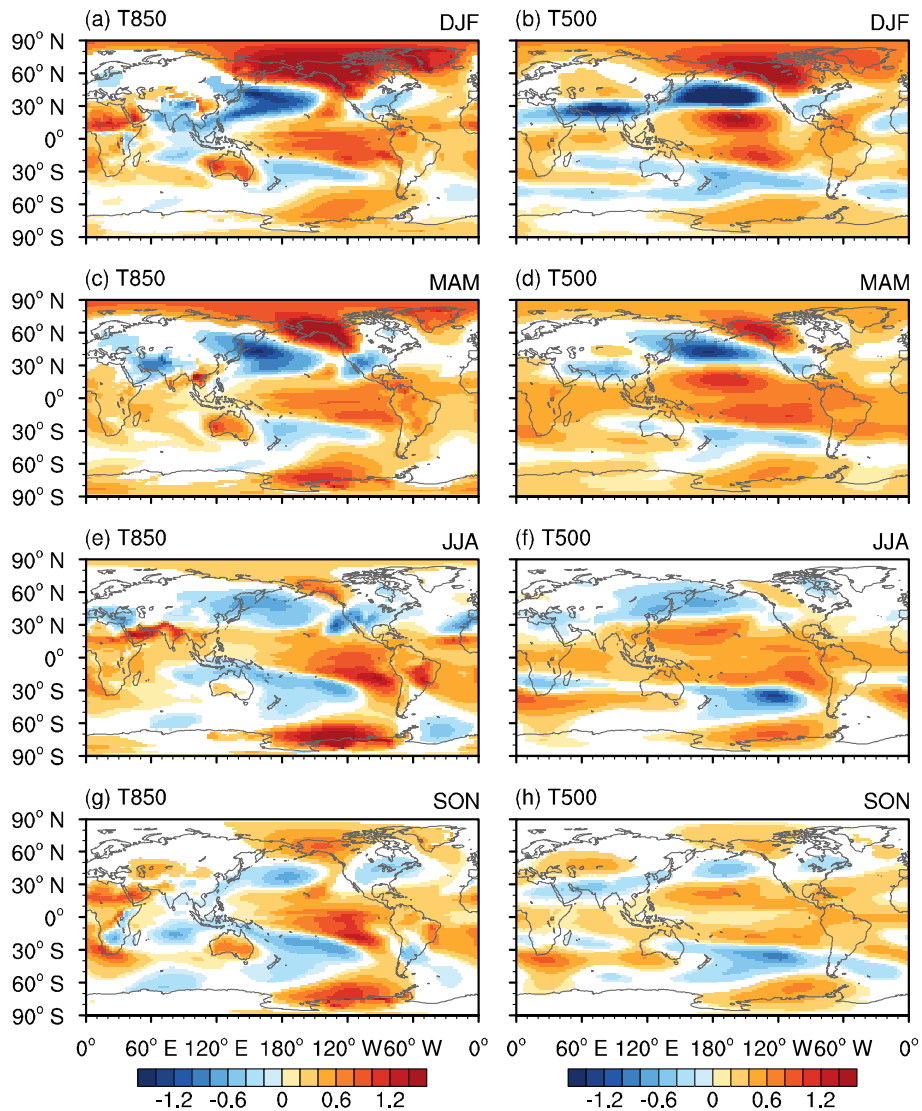
Figure 4. Simulated seasonal temperature anomalies during the positive phases of the IPO. Regressed maps of 850 hPa temperature anomalies (units: °C) in **(a)** winter, **(c)** spring, **(e)** summer, and **(g)** autumn onto the time series of the IPO index simulated by multiple members of the CESM-LME all-forcing runs. **(b)** Winter, **(d)** spring, **(f)** summer, and **(h)** autumn for 500 hPa temperature anomalies (units: °C). Shading shows that at least two-thirds of the members simulate significant changes (at the 95% significance level), and these significant changes agree on the sign of the average of multiple members.

3.3.1 Arid central Asia

304   In spring, warming appeared over the northern low and high latitudes, whereas

305   cooling appeared over the northern mid-latitudes, especially in the eastern hemisphere,

306   corresponding to a positive phase of the IPO (Fig. 4c and 4d). The tropospheric

307   temperature anomalies led to an enhanced (weakened) meridional temperature

308   gradient over low (high) latitudes as the climatological temperature decreased from

309   low to high latitudes. The anomalies in the temperature gradient contributed to

310   enhanced westerlies over low latitudes and weakened westerlies over high latitudes

311   via the thermal wind relation (Fig. 5c and 5d), indicating a southward shift of the

312   mid-latitude westerlies. The enhanced westerlies over the Mediterranean Sea and to

313   its east transported more water vapor from the Mediterranean Sea to southern central

314   Asia (Fig. 5a).

315   Positive sea-level pressure (SLP) anomalies appeared over the Indo–western

316   Pacific warm pool and negative SLP anomalies appeared over the eastern tropical

317   Pacific (Fig. 5c), consistent with the SST anomalies during positive IPO phases. The

318   distribution of the SLP anomalies indicated a weakened Walker circulation over the

319   Pacific Ocean, which further led to suppressed convection over the maritime continent

320   (Li et al., 2022). The decreased latent heating associated with the decreased

321   precipitation over the maritime continent can produce westward-propagating

322   baroclinic Rossby wave trains (Jiang et al., 2021). This resulted in anomalous

323   low-level anticyclone and upper-level cyclone over the Indian subcontinent, both of

324   which led to anomalous southerlies over central Asia (Fig. 5c and 5d). The anomalous

325   southerlies induced warm advection and led to anomalous ascending motion in this

326 region (Fig. 5b). In addition, the anomalous southerlies at low troposphere also could

327 transport more water vapor from low latitudes to central Asia (Fig. 5a). The enhanced

328 transport of water vapor and the anomalous ascending motion both favored increased

329 precipitation in spring over central Asia. In summary, the IPO affected the

330 precipitation from westerly winds through modulating the mid-latitude westerlies and

331 the Walker circulation in the Pacific Ocean.
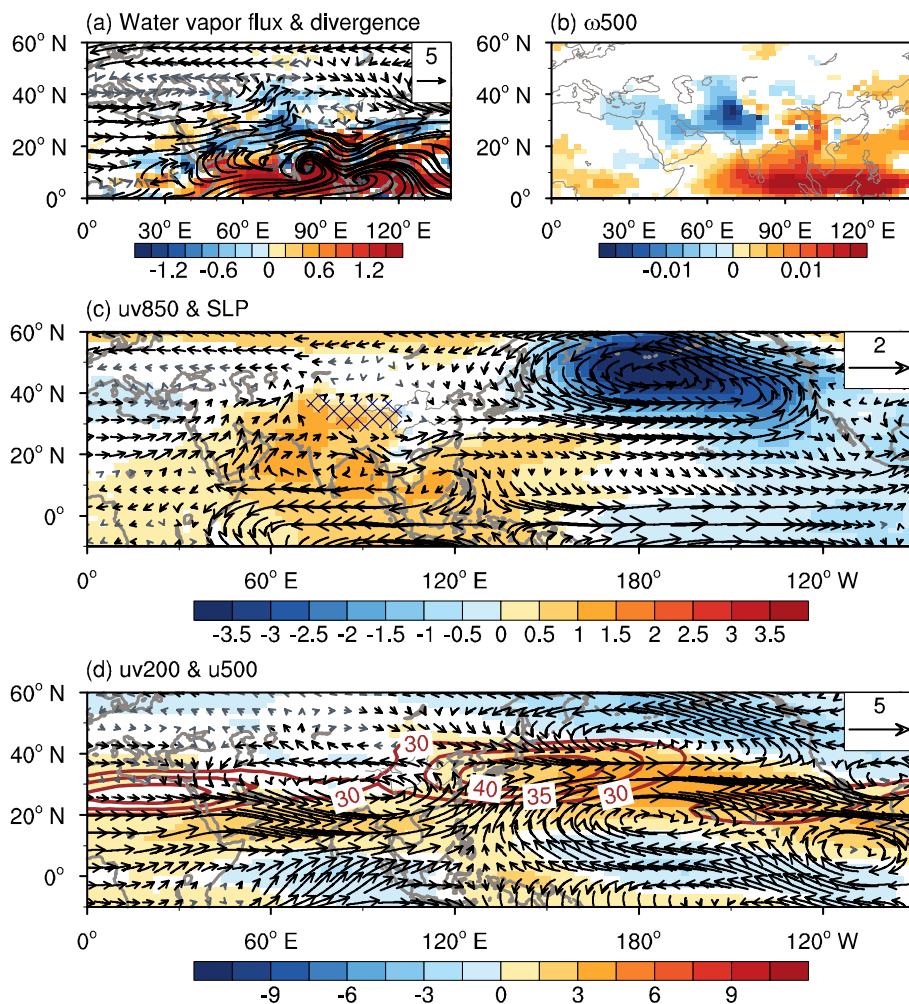
332

333 **Figure 5.** Simulated spring atmospheric circulation anomalies during the positive phases of the

334 IPO. Regressed maps of anomalous **(a)** vertically integrated water vapor flux from 1000 to 300

335 hPa (vectors; units: kg m^{-1} s^{-1}) and its divergence (shading; units: 10^{-5} kg m^{-2} s^{-1}), **(b)** 500 hPa

336 vertical velocity (ω500) (units: Pa s^{-1}), **(c)** 850 hPa wind (uv850) (vectors; units: m s^{-1}) and SLP

337 (shading; units: hPa), **(d)** 200 hPa wind (uv200) (vectors; units: m s^{-1}) and 500 hPa zonal wind

338 (u500) (shading; units: m s^{-1}) onto the time series of the IPO index simulated by the CESM-LME

339 all-forcing runs. The blue hatched patterns in part **(c)** indicate the region with an altitude >3000 m.

340 The brown contours in part **(d)** are the climatological 200 hPa zonal wind (units: m s^{-1}). The

341 shading shows that at least two-thirds of the members simulate significant changes (at the 95%

342 significance level), and these significant changes agree on the sign of the average of multiple

343 members. The black vectors show that for the zonal or meridional component, at least two-thirds

344 of the members simulate significant changes (at the 95% significance level), and these significant

345 changes agree on the sign of the average.

346   The circulation anomalies associated with the IPO in winter were similar to those

347 in spring (Fig. S6), indicating that the processes by which the IPO modulated winter

348 precipitation in central Asia were similar to those in spring.

349 **3.3.2 Asian monsoon regions**

350   In summer, higher (lower) SLPs appeared over the most of the Asian continent

351 (northern Pacific) during the positive phases of the IPO (Fig. 6c). This was the reverse

352 of the climatological state, in which the SLP over most of the Asian continent was

353 lower than that over the neighboring oceans. A weakened land–sea thermal contrast

354 was therefore induced. The weakened land–sea thermal contrast led to a weakened

355 Asian summer monsoon (ASM), featured by northerly anomalies at 850 hPa over the

356 whole of monsoonal Asia (Fig. 6c). The northerly anomalies further led to weakened

357 water vapor transport in this region (Fig. 6a).

358   Anomalies also appeared in the tropospheric temperature (Fig. 4e and 4f) and

359 caused westerly (easterly) anomalies over the south (north) of the climatological

360 Asian subtropical westerly jet at 200 hPa (Fig. 6d). The wind anomalies indicated the

361 southward shift in the Asian subtropical westerly jet and the associated secondary

362 meridional–vertical circulation (Cressman, 1981; Ding, 2005; Zhang and Huang,

363 2011), which led to anomalous downward motion over northern China and anomalous

364 upward motion over southern China (Fig. 6b) (Wang et al., 2013; Zhu et al., 2015).

365 The western Pacific subtropical high shifted southeastward (Fig. 6d), which did not

366 favor the transport of water vapor to northern China (Fig. 6a). These circulation

367 anomalies all indicate a weakened ASM system (Webster and Yang, 1992; Wang,

368 2001). Precipitation over southern China therefore increased in summer, whereas

369 precipitation over northern China and most of the South Asian monsoon regions

370 decreased. In summary, the IPO affected the monsoon precipitation through

371 modulating the ASM system.
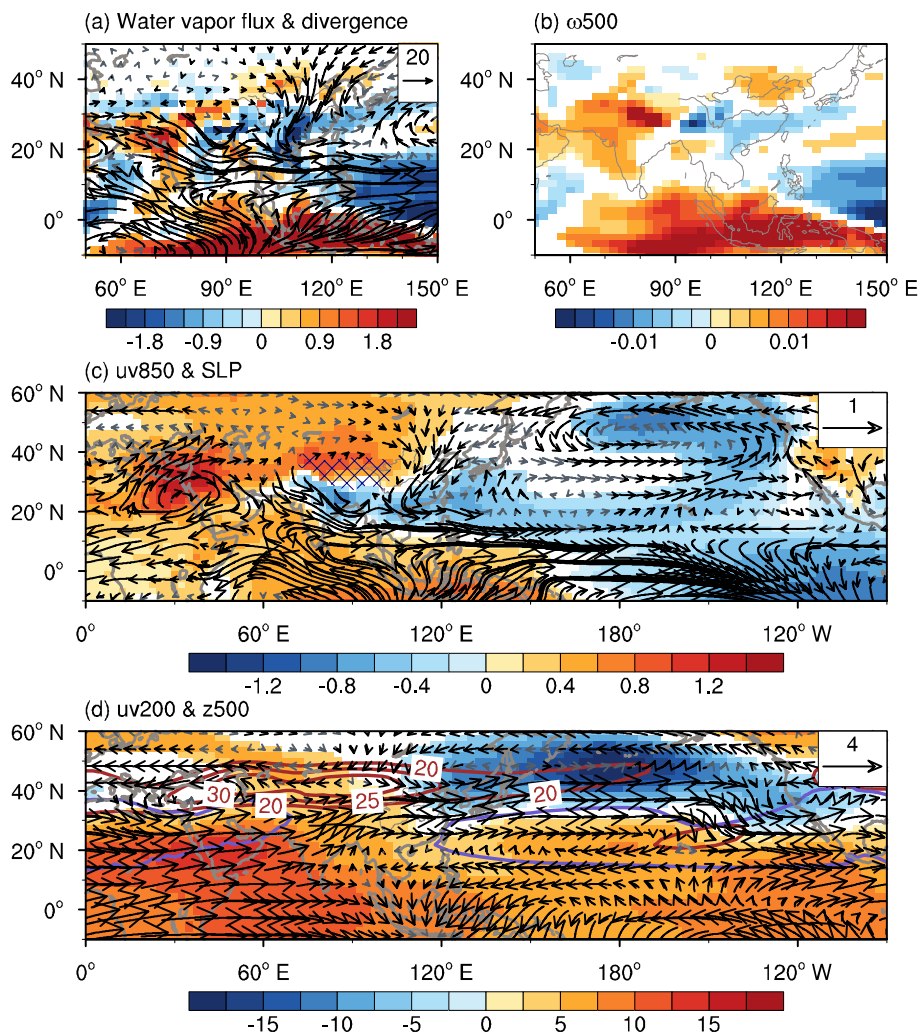
372

373 **Figure 6.** Simulated summer atmospheric circulation anomalies during the positive phases of the

374   IPO. Regressed maps of anomalous **(a)** vertically integrated water vapor flux from 1000 to 300

375   hPa (vectors; units: kg m^{-1} s^{-1}) and its divergence (shading; units: 10^{-5} kg m^{-2} s^{-1}), **(b)** 500 hPa

376   vertical velocity (ω500) (units: Pa s^{-1}), **(c)** 850 hPa wind (uv850) (vectors; units: m s^{-1}) and SLP

377   (shading; units: hPa), and **(d)** 200 hPa wind (uv200) (vectors; units: m s^{-1}) and 500 hPa

378   geopotential height (z500) (shading; units: m) onto the time series of the IPO index simulated by

379   the CESM-LME all-forcing runs. The blue hatched patterns in part **(c)** indicate the region with an

380   altitude >3000 m. The brown contours in part **(d)** are the climatological 200 hPa zonal wind (units:

381   m s^{-1}). The purple line in part **(d)** is the isoline with a value of 5860 m in the climatology state.

382   The shading shows that at least two-thirds of the members simulate significant changes (at the 95%

383   significance level), and these significant changes agree on the sign of the average of multiple

384   members. The black vectors show that for the zonal or meridional component, at least two-thirds

385   of the members simulate significant changes (at the 95% significance level), and these significant

386   changes agree on the sign of the average.

387   In autumn, negative anomalies in the 500 hPa geopotential height appeared over

388   the Korean Peninsula (Fig. S7d), indicating a strengthened East Asian trough (EAT)

389   during the positive phases of the IPO (Qin et al., 2018, 2020; Li et al., 2020). The

390   strengthened EAT contributed to northerly anomalies over East Asia (Fig. S7c), which

391   led to weakened water vapor transport in this region (Fig. S7a). The anomalous

392   northerlies to the west of the strengthened EAT induced cold advection (Fig. S7c and

393   S7d) and led to anomalous descending motion over northern China (Fig. S7b).

394   Precipitation therefore decreased over northern China in autumn.

395   Consistent with the SST anomalies during the positive phases of the IPO,

396   positive (negative) SLP anomalies appeared over the Indo–western Pacific warm pool

397   (eastern tropical Pacific) in all four seasons (Figs. 5c, 6c, S6c and S7c), indicating a

398   weakened Walker circulation in the Pacific Ocean, which is in agreement with the

399 results in Dong and Lu (2013) and Zhao et al. (2021). This weakened Walker

400 circulation contributed to decreased precipitation over most of the South Asian

401 monsoon regions (Krishnamurthy and Krishnamurthy, 2014; Li et al., 2021).

3.4 Decisive role of internal variability

403 Many studies have suggested that both external forcings and internal variability

404 could affect the decadal variability of precipitation over Asia (e.g., Wang et al., 2013;

405 Jin et al., 2019; Zhu et al., 2022). To identify the roles of internal variability and

406 external forcing, Fig. 7 shows the first leading decadal precipitation modes of the

407 control and single-forcing simulations. The decadal linkage between the changes in

408 precipitation pattern in central Asia and monsoonal Asia in the all-forcing simulations

409 also appeared in the control simulation (Fig. 7a), implying this decadal linkage was

410 mainly caused by the internal variability. Nearly all the single-forcing simulations

411 presented similar decadal linkage with all-forcing simulations, apart from the

412 simulations forced by ozone and aerosols (Fig. 7b–g). This indicated that, during the

413 last millennium, volcanic eruptions, solar activity, greenhouse gases, land use and

414 land cover, and the Earth's orbit were unable to change the decadal linkage between

415 the changes in precipitation pattern in arid regions and monsoon regions in Asia,

416 which was dominated by the internal variability. Only in the ozone and aerosols

417 forcing simulations, which covered the period of 1850–2005, the decadal linkage of

418 precipitation changes disappeared. We further examined the results of other forcing

419 simulations for the period of 1850–2005 (Fig. S8), and all the first decadal

420 precipitation modes simulated by other forcing experiments still indicated similar

421 decadal linkage with all-forcing last-millennium simulations. This meant that since

422 the industrial revolution, only the ozone and aerosol forcing factors can change the

423 dominant mode of the reverse variation of precipitation in East Asia from north to

424 south and present stronger local climate effects. As noted by Wang et al. (2013), it

425 may be that anthropogenic aerosols play a more important role in regulating

426 precipitation in East Asia, which needs further analysis.

427
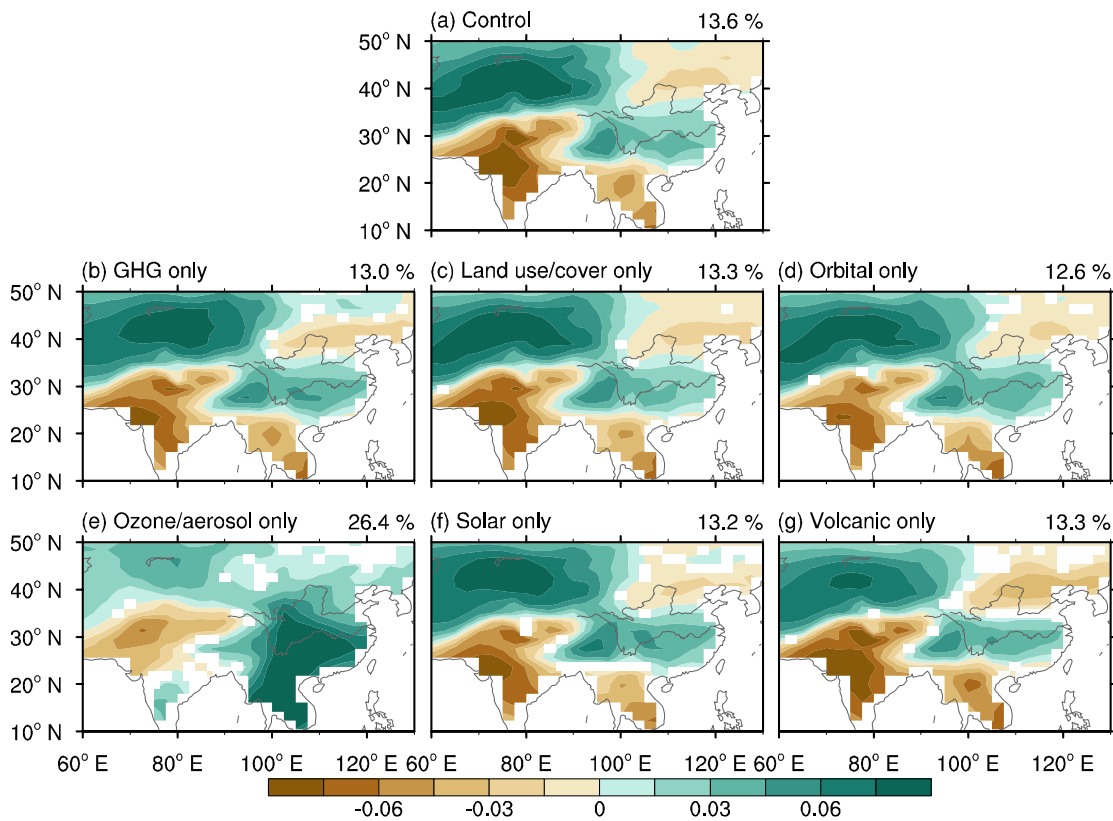
Figure 7. The leading decadal precipitation mode for the time period 850–2005 in the control and

single-forcing simulations, with the exception of leading mode for the time period 1850–2005 in

experiment forced by ozone and aerosols. **(a)** EOF1 of the nine-year low-pass Lanczos filtered

annual precipitation in the control simulation. The explained variance is given at the top-right. **(b–**

g) The average EOF1 of the nine-year low-pass Lanczos filtered annual precipitation in six subsets

of the single-forcing simulations: a subset of three simulations forced by greenhouse gas

emissions (GHG); a subset of three simulations forced by land use and land cover; a subset of

three simulations forced by the Earth's orbit; a subset of four simulations forced by ozone and

436   aerosols; a subset of four simulations forced by solar activity; and a subset of five simulations

437   forced by volcanic eruptions. The averaged explained variance is given at the top-right. The

438   shading in parts **(b–g)** shows where at least two-thirds of the members agree on the sign of the

439   average of multiple members.

440   Apart from the simulations forced by ozone and aerosols, the SST anomalies

441   associated with the leading precipitation mode in the control and single-forcing

442   simulations all showed a positive IPO pattern (Fig. S9), consistent with the all-forcing

443   simulations. At the same time, the precipitation anomalies associated with the positive

444   IPO in the control and single-forcing simulations all showed positive anomalies in

445   arid central Asia and southern China and negative anomalies in the South Asian

446   monsoon region and most of northern China (Fig. 8), also consistent with the

447   all-forcing simulations. This suggested that these external forcing factors cannot

448   change the dominant influence of IPO on Asian decadal precipitation and lead to the

449   decadal linkage between the changes in precipitation pattern in arid regions and

450   monsoon regions in Asia during the last millennium. It is therefore clear that the

451   internal variability associated with the IPO had a decisive role in shaping the decadal

452   linkage of precipitation changes.
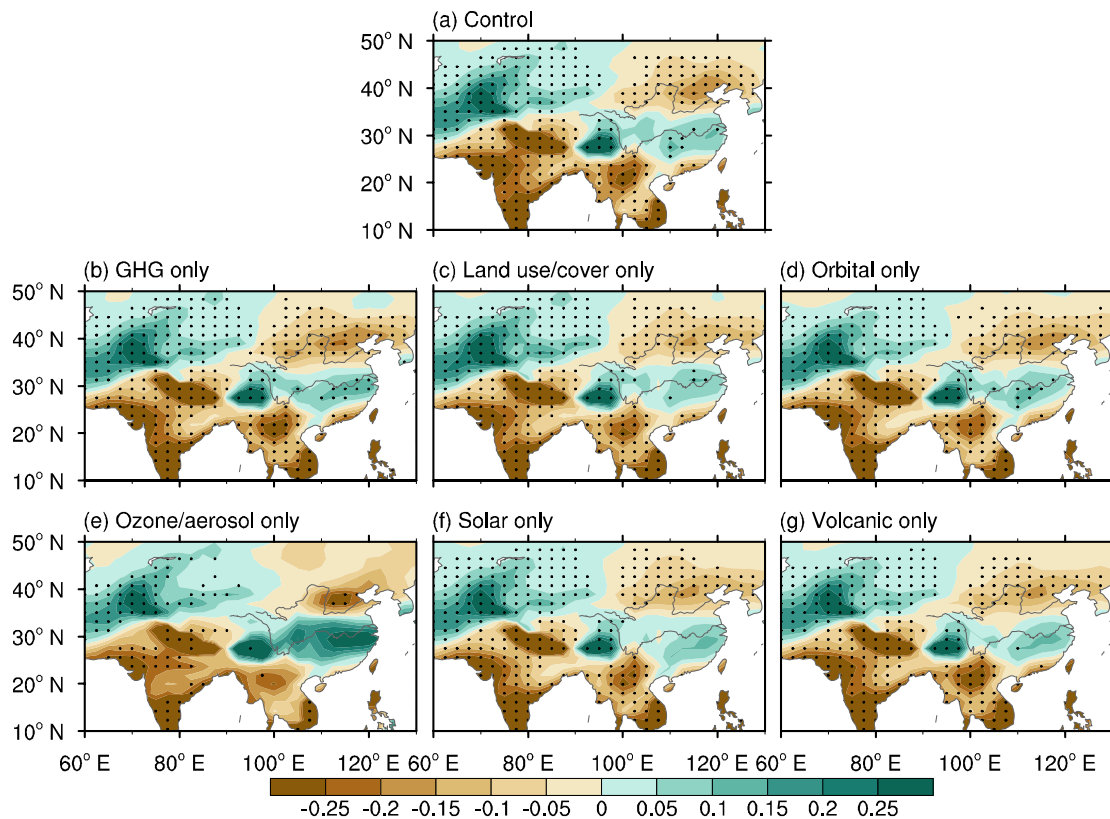
Figure 8. Simulated precipitation anomalies during the positive phases of the IPO in the control and single-forcing simulations. **(a)** Precipitation anomalies (units: mm day^{-1}) regressed onto the time series of the IPO index in the control run. **(b–g)** Precipitation anomalies (units: mm day^{-1}) regressed onto the time series of the IPO index in six subsets of the single-forcing simulations. The dots in part (a) show significant anomalies at the 95% confidence level and the dots in parts (b–g) denote that at least two-thirds of the members simulate significant changes (at the 95% significance level), and these significant changes agree on the sign of the average of multiple members.

In the ozone and aerosols forcing simulations, we can find positive precipitation anomalies in arid central Asia and southern China and negative precipitation anomalies in the South Asian monsoon region and most of northern China during the positive phases of the IPO (Fig. 8e). However, the changes in East Asian precipitation were no longer significant, which meant that the impacts of IPO on East Asian precipitation in this experiment were weakened.

3.5 Simulated first leading moisture mode

Terrestrial moisture conditions are closely related to precipitation changes and could strongly affect terrestrial ecosystems. The terrestrial moisture condition is quantified by both aridity index and soil moisture content here. Based on our analyses of the aridity index (Fig. 9a) and the soil moisture content (Fig. S10a), we found that the EOF1 of the decadal changes in Asian moisture during the last millennium also showed the same changes in moisture in arid central Asia and southern China, which were the opposite of those in the South Asian monsoon region and most of northern China. This is consistent with the first leading precipitation mode, suggesting the important contribution of precipitation to the decadal linkage between the changes in moisture pattern in arid regions and monsoon regions in Asia. Similar first leading moisture mode was seen in all the experiments apart from those with only ozone and aerosol forcing (Figs. 9 and S10), indicating the decisive role of internal variability on the decadal linkage of moisture changes.
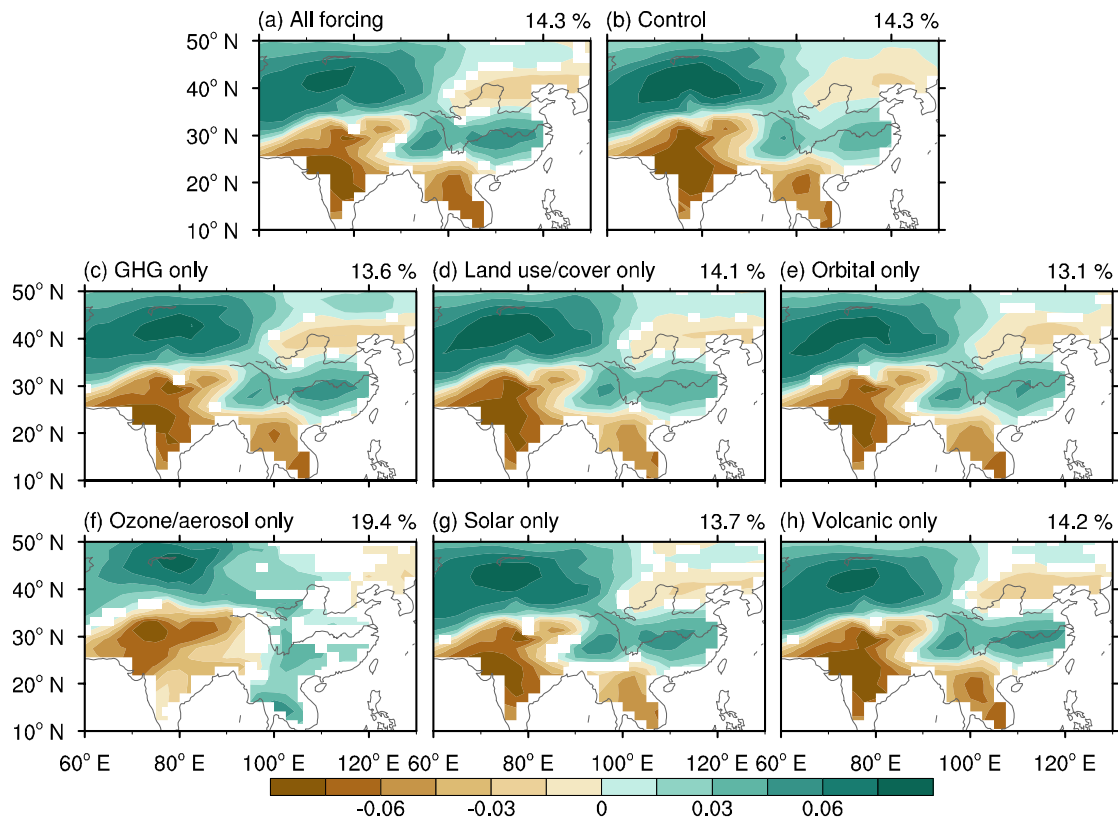
Figure 9. The simulated leading decadal aridity index mode for the time period 850–2005 in all the experiments, with the exception of leading mode for the time period 1850–2005 in experiment forced by ozone and aerosols. **(a)** The average EOF1 of the nine-year low-pass Lanczos filtered aridity index in the all-forcing simulations. The averaged explained variance is given at the top-right. **(b)** EOF1 of the nine-year low-pass Lanczos filtered aridity index in the control simulation. The explained variance is given at the top-right. **(c–h)** The average EOF1 of the nine-year low-pass Lanczos filtered aridity index in six subsets of the single-forcing simulations. The averaged explained variance is given at the top-right. The shading in parts **(a, c–h)** shows where at least two-thirds of the members agree on the sign of the average of multiple members.

The SST anomalies associated with the leading moisture mode in all experiments, apart from those with only ozone and aerosol forcing, showed a positive IPO pattern (Figs. S11 and S12), indicating the dominant role of the IPO on the decadal linkage of moisture changes. The moisture anomalies associated with the positive IPO showed positive anomalies in arid central Asia and southern China and negative anomalies in

497 the South Asian monsoon region and most of northern China in all the experiments

498 (Figs. 10 and S13), consistent with the leading moisture mode. This further confirmed

499 the aforementioned dominant role of the IPO. Therefore, the internal variability

500 associated with the IPO also had a decisive role in shaping the decadal linkage

501 between the changes in moisture pattern in arid regions and monsoon regions in Asia

502 through regulating precipitation during the last millennium.
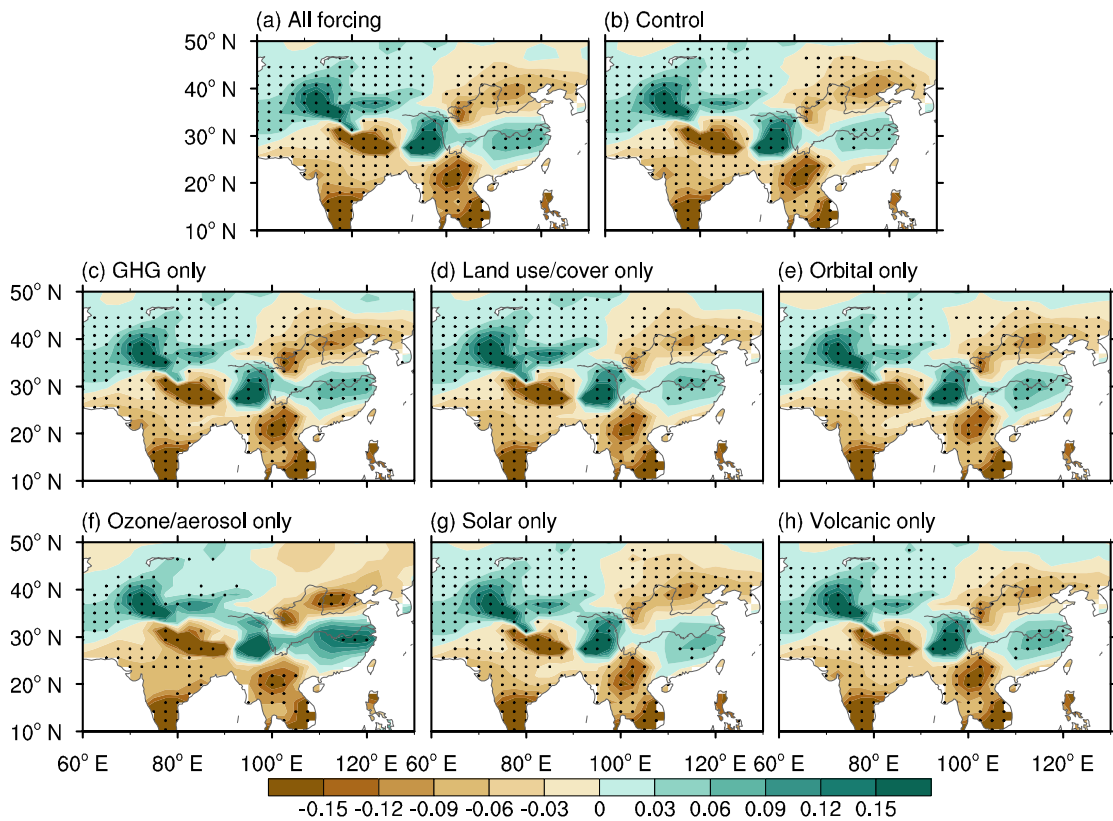
504 **Figure 10.** Simulated aridity index anomalies during the positive phases of the IPO. The aridity

505 index anomalies regressed onto the time series of the IPO index in the **(a)** all-forcing simulations,

506 **(b)** control simulation, and **(c–h)** six subsets of the single-forcing simulations. The dots in part **(b)**

507 show significant anomalies at the 95% confidence level and the dots in parts **(a, c–h)** denote that

508 at least two-thirds of the members simulate significant changes (at the 95% significance level),

509 and these significant changes agree on the sign of the average of multiple members.

510 **4 Discussion**

4.1 Limited impacts of external forcings on decadal precipitation linkage

As stated in section 3.4, the spatial pattern of leading decadal precipitation mode in all-forcing simulations also appears in control and all single-forcing simulations, apart from the simulations forced by ozone and aerosols. This indicates the dominant role of internal variability in shaping the spatial pattern of leading decadal precipitation mode during the last millennium. Moreover, this process can be partially influenced by the impacts of ozone and aerosol forcing since the industrial revolution. During this period, ozone and aerosols have played crucial roles in regulating the climate at mid-latitudes in the Northern Hemisphere (Miao et al., 2022). However, the relative impact of internal variability and external forcings on the time variations of the leading decadal precipitation mode during the last millennium remains unclear. Thus, we calculated the correlations across the time series of the leading decadal precipitation mode (i.e., the principal components) simulated by CESM-LME 12 all-forcing simulations (Table S1). Except for autocorrelations for each principal component, the other correlations range from -0.06 to 0.35, and only 13.6% correlations are significant at the 95% confidence level. These relatively small correlations indicate the impacts of external forcings on the time variations of the leading decadal precipitation mode are very weak. The several significant correlations suggest that, to a limited extent, the time variations of the leading decadal precipitation mode could be affected by external forcings (e.g., volcanic eruptions and solar radiation) (Ning et al., 2020; Xue et al., 2023). Therefore, internal variability played a dominant role in shaping the time variations of the leading decadal

533   precipitation mode.

534   In summary, the impacts of external forcings on both spatial pattern and time

535   variations of the leading decadal precipitation mode are relatively weak, which

536   indicates limited impacts of external forcings on decadal linkage between

537   precipitation changes in arid central Asia and humid monsoonal Asia during the last

538   millennium. This is quite different from the dominating role of external forcings in

539   regulating the variations of Asian precipitation at suborbital and longer timescales (Xu

540   et al., 2023).

541   **4.2 Centennial precipitation/moisture linkage**

542   The features of decadal linkage between moisture/precipitation changes in arid

543   central Asia and humid monsoonal Asia during the last millennium have been

544   investigated and the dynamic mechanisms associated with the decadal linkage have

545   been explored above. Next, the potential linkage on multi-centennial scale implied by

546   reconstruction is discussed here. Between the LIA and MCA, on multi-centennial

547   scale, wetter (drier) conditions over arid central Asia and southern China (most of

548   northern China) were reconstructed in Chen et al. (2015) (Fig. 11a). Besides, the

549   changes in precipitation between the LIA and the MCA based on the LMR showed

550   more (less) precipitation over eastern central Asia and southern China (the South

551   Asian monsoon region and most of northern China) (Fig. 11a), consistent with the

552   reconstructed changes in precipitation/moisture in Chen et al. (2015). These results

553   suggest a robust centennial linkage of the changes in precipitation/moisture in central

554   Asia and monsoonal Asia, similar to the decadal precipitation/moisture linkage.
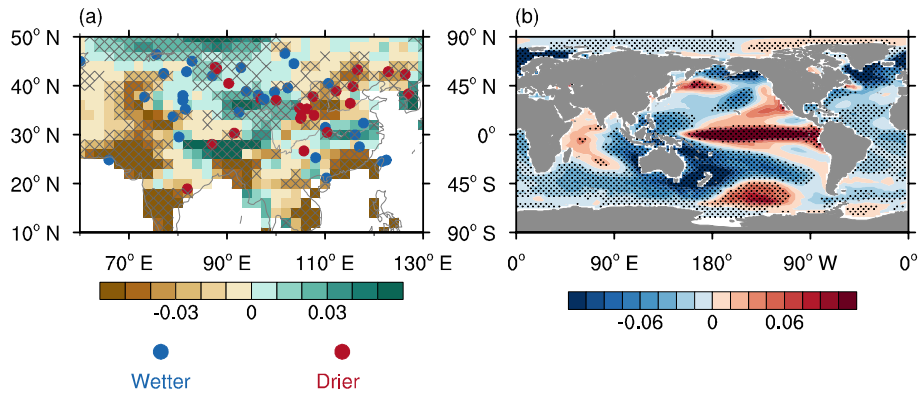
Figure 11. Reconstructed changes in **(a)** precipitation (units: mm day^{-1}) and **(b)** SST (units: °C) between the LIA and MCA in the LMR. The gray hatched patterns in part **(a)** and black dots in part **(b)** indicate significant anomalies at the 95% confidence level. The dots in part **(a)** represent the reconstructed precipitation/moisture records modified from Chen et al. (2015); the blue (red) dots denote wetter (drier) conditions in the LIA than in the MCA.

The reconstructed changes in the SST between the LIA and MCA showed higher (lower) SSTs over the central-eastern equatorial Pacific (the western-central parts of both the subtropical North Pacific and South Pacific) (Fig. 11b). According to the present study, the IPO-like condition may be the primary cause of the centennial linkage of changes in precipitation/moisture in central Asia and monsoonal Asia. However, most current models still cannot reproduce the evolution of the Pacific Decadal Oscillation (Wang and Miao, 2018). The CESM-LME simulations were also unable to produce the reconstructed centennial changes in SST between the LIA and MCA. Therefore, in the present study, we cannot directly obtain the evidence of the aforementioned centennial linkage from the CESM-LME results. The failure of CESM-LME simulations in reproducing the centennial linkage further limits our understanding of the relative roles of the external forcings and internal variability in shaping the centennial linkage. Thus, further investigation remains needed.

5 Conclusions

Based on the LMR dataset and CESM-LME all-forcing simulations, the first leading precipitation mode in Asia on decadal scale during the last millennium showed the same changes in precipitation in arid central Asia and southern China, which were the opposite of those in the South Asian monsoon region and most of northern China. This mode indicated a robust linkage between the changes in precipitation pattern in arid regions and monsoon regions in Asia on decadal scale, in which the evolution of precipitation in central Asia was out-of-phase with that of northern China and the South Asian monsoon regions and in-phase with that of southern China.

Further analysis based on CESM-LME all-forcing, control and all single-forcing simulations showed that the internal variability associated with the IPO plays a dominant role in connecting the decadal variations in precipitation between arid central Asia and monsoonal Asia by modulating the precipitation of their respective major rainy seasons during the last millennium. In spring, the positive IPO could enhance westerlies over the Mediterranean Sea and to its east, which could transport more water vapor and cause increased precipitation over central Asia. In summer, the positive IPO is accompanied with weakened Asian summer monsoon and southward Asian subtropical westerly jet, which further lead to increased (decreased) summer precipitation over southern China (over northern China and South Asian monsoon region). Besides, the positive IPO can weaken Pacific Walker circulation, which contributes to precipitation decrease over South Asian monsoon regions in all four

596 seasons.

597   In addition, this decadal linkage of precipitation variation also causes a similar

598 decadal linkage of moisture changes in central Asia and monsoonal Asia during the

599 last millennium.

600

601 **Data availability.** The Last Millennium Reanalysis (LMR) Version 2.1 dataset (Tardif

602 et al., 2019; Anderson et al., 2019) used in this study are available at

603 https://www.atmos.uw.edu/~hakim/LMR/. The Community Earth System Model-Last

604 Millennium Ensemble (CESM-LME) (Otto-Bliesner et al., 2016) can be founded at

605 https://www.cesm.ucar.edu/community-projects/lme.

606

607 **Author contributions**. TW designed the study; HX analyzed the dataset and plotted

608 the figures; HX, TW and HW all contributed to writing the manuscript and

609 interpreting results; Funding was acquired by TW and HX.

610

611 **Competing interests.** The authors declare that they have no conflict of interest.

612

613 **Acknowledgements.** We sincerely thank two anonymous reviewers and editor for

614 their valuable comments and suggestions, which helped to improve the quality of this

615 paper significantly. This research has been supported by the National Natural Science

616 Foundation of China (Grant No. 42221004), the National Key Research and

617 Development Program of China (Grant No. 2018YFA0606403), and the Postgraduate

618   Research and Practice Innovation Program of Jiangsu Province (KYCX21_0944).

619

620   **References**

621   Aizen, E. M., Aizen, V. B., Melack, J. M., Nakamura, T., and Ohta, T.: Precipitation

622   and atmospheric circulation patterns at mid-latitudes of Asia, Int. J. Climatol., 21,

623   535–556, https://doi.org/10.1002/joc.626, 2001.

624   Allen,   R.   G.,   Pereira,   L.   S.,   Raes,   D.,   and   Smith,   M.:   Crop

625   evapotranspiration-guidelines for computing crop water requirements, Food and

626   Agriculture Organization of the United Nations Irrigation and Drainage Paper 56,

627   1–326, 1998.

628   Anderson, D. M., Tardif, R., Horlick, K., Erb, M. P., Hakim, G. J., Noone, D., Perkins,

629   W. A., and Steig, E.: Additions to the Last Millennium Reanalysis multi-proxy

630   database, Data Science Journal, 18, 1–11, http://doi.org/10.5334/dsj-2019-002,

631   2019.

632   Bretherton, C. S., Widmann, M., Dymnikov, V. P., Wallace, J. M., and Bladé, I.: The

633   effective number of spatial degrees of freedom of a time-varying field, J. Climate,

634   12,   1990–2009,

635   https://doi.org/10.1175/1520-0442(1999)012<1990:tenosd>2.0.co;2, 1999.

636   Chen, F., Chen, J., Holmes, J., Boomer, I., Austin, P., Gates, J. B., Wang, N., Brooks,

637   S. J., and Zhang, J.: Moisture changes over the last millennium in arid central

638   Asia: a review, synthesis and comparison with monsoon region, Quaternary Sci.

639   Rev., 29, 1055–1068, https://doi.org/10.1016/j.quascirev.2010.01.005, 2010.

640   Chen, F., Huang, W., Jin, L., Chen, J., and Wang, J.: Spatiotemporal precipitation

641   variations in the arid Central Asia in the context of global warming, Sci. China

642   Earth Sci., 54, 1812–1821, https://doi.org/10.1007/s11430-011-4333-8, 2011.

643   Chen, J., Chen, F., Feng, S., Huang, W., Liu, J., and Zhou, A.: Hydroclimatic changes

644   in China and surroundings during the Medieval Climate Anomaly and Little Ice

645   Age: spatial patterns and possible mechanisms, Quaternary Sci. Rev., 107, 98–

646   111, https://doi.org/10.1016/j.quascirev.2014.10.012, 2015.

647   Chu, C., Yang, X.-Q., Sun, X., Yang, D., Jiang, Y., Feng, T., and Liang, J.: Effect of

648   the tropical Pacific and Indian Ocean warming since the late 1970s on wintertime

649   Northern Hemispheric atmospheric circulation and East Asian climate

650   interdecadal changes, Clim. Dynam., 50, 3031–3048,

651   https://doi.org/10.1007/s00382-017-3790-y, 2018.

652   Cressman, G. P.: Circulations of the west Pacific jet stream, Mon. Weather Rev., 109,

653   2450–2463, https://doi.org/10.1175/1520-0493(1981)109<2450:cotwpj>2.0.co;2,

654   1981.

655   Ding, Y.: Advanced synoptic meteorology, China Meteorological Press, Beijing, 2005.

656   Ding, Y. and Chan, J. C. L.: The East Asian summer monsoon: an overview, Meteorol.

657   Atmos. Phys., 89, 117–142, https://doi.org/10.1007/s00703-005-0125-z, 2005.

658   Ding, Y., Wang, Z., and Sun, Y.: Inter-decadal variation of the summer precipitation in

659   East China and its association with decreasing Asian summer monsoon. Part I:

660   Observed evidences, Int. J. Climatol., 28, 1139–1161,

661   https://doi.org/10.1002/joc.1615, 2008.

662 Dong, B. and Lu, R.: Interdecadal enhancement of the walker circulation over the

663   Tropical Pacific in the late 1990s, Adv. Atmos. Sci., 30, 247–262,

664   https://doi.org/10.1007/s00376-012-2069-9, 2013.

665 Gilman, D. L., Fuglister, F. J., and Mitchell, J. M.: On the power spectrum of "red

666   noise",   J.   Atmos.   Sci.,   20,   182–184,

667   https://doi.org/10.1175/1520-0469(1963)020<0182:otpson>2.0.co;2, 1963.

668 Henley, B. J., Gergis, J., Karoly, D. J., Power, S., Kennedy, J., and Folland, C. K.: A

669   Tripole Index for the Interdecadal Pacific Oscillation, Clim. Dynam., 45, 3077–

670   3090, https://doi.org/10.1007/s00382-015-2525-1, 2015.

671 Hu, Y., Sun, W., Liu, J., Chen, D., Ning, L., and Peng, Z.: Decadal variability of

672   precipitation over the Tibetan Plateau modulated by the 11-year solar cycle over

673   the   past   millennium,   Front.   Earth   Sci.,   11,

674   https://doi.org/10.3389/feart.2023.1137205, 2023.

675 Huang, J., Ma, J., Guan, X., Li, Y., and He, Y.: Progress in semi-arid climate change

676   studies   in   China,   Adv.   Atmos.   Sci.,   36,   922–937,

677   https://doi.org/10.1007/s00376-018-8200-9, 2019.

678 Huang, W., Chen, F., Feng, S., Chen, J., and Zhang, X.: Interannual precipitation

679   variations   in   the   mid-latitude   Asia   and   their   association   with   large-scale

680   atmospheric   circulation,   Chinese   Sci.   Bull.,   58,   3962–3968,

681   https://doi.org/10.1007/s11434-013-5970-4, 2013.

682 Huang, W., Chen, J., Zhang, X., Feng, S., and Chen, F.: Definition of the core zone of

683   the "westerlies-dominated climatic regime", and its controlling factors during the

instrumental period, Sci. China Earth Sci., 58, 676–684, https://doi.org/10.1007/s11430-015-5057-y, 2015.

Hurrell, J. W., Holland, M. M., Gent, P. R., Ghan, S., Kay, J. E., Kushner, P. J., Lamarque, J.-F., Large, W. G., Lawrence, D., Lindsay, K., Lipscomb, W. H., Long, M. C., Mahowald, N., Marsh, D. R., Neale, R. B., Rasch, P., Vavrus, S., Vertenstein, M., Bader, D., Collins, W. D., Hack, J. J., Kiehl, J., and Marshall, S.: The Community Earth System Model: A framework for collaborative research, B. Am. Meteorol. Soc., 94, 1339–1360, https://doi.org/10.1175/bams-d-12-00121.1, 2013.

Jiang, D., Su, M., Wei, R., and Bao, L.: Variation and projection of drought and wet conditions in Xinjiang, Chinese Journal of Atmospheric Sciences, 33, 90–98, https://doi.org/10.3878/j.issn.1006-9895.2009.01.08, 2009.

Jiang, J., Zhou, T., Chen, X., and Wu, B.: Central Asian precipitation shaped by the tropical Pacific Decadal Variability and the Atlantic Multidecadal Variability, J. Climate, 34, 7541–7553, https://doi.org/10.1175/jcli-d-20-0905.1, 2021.

Jin, C., Liu, J., Wang, B., Yan, M., and Ning, L.: Decadal variations of the East Asian summer monsoon forced by the 11-year insolation cycle, J. Climate, 32, 2735–2745, https://doi.org/10.1175/jcli-d-18-0288.1, 2019.

Krishnamurthy, L. and Krishnamurthy, V.: Influence of PDO on South Asian summer monsoon and monsoon–ENSO relation, Clim. Dynam., 42, 2397–2410, https://doi.org/10.1007/s00382-013-1856-z, 2014.

Li, B., Li, Y., Chen, Y., Zhang, B., and Shi, X.: Recent fall Eurasian cooling linked to

706   North Pacific sea surface temperatures and a strengthening Siberian high, Nat.

707   Commun., 11, 5202, https://doi.org/10.1038/s41467-020-19014-2, 2020.

708 Li, G., Gao, C., Lu, B., and Chen, H.: Inter-annual variability of spring precipitation

709   over the Indo-China Peninsula and its asymmetric relationship with El

710   Niño-Southern Oscillation, Clim. Dynam., 56, 2651–2665,

711   https://doi.org/10.1007/s00382-020-05609-4, 2021.

712 Li, T., Wang, Y., Wang, B., Ting, M., Ding, Y., Sun, Y., He, C., and Yang, G.:

713   Distinctive South and East Asian monsoon circulation responses to global

714   warming, Sci. Bull., 67, 762–770, https://doi.org/10.1016/j.scib.2021.12.001,

715   2022.

716 Miao, J., Wang, T., and Jiang, D.: Ozone-aerosol and land use reversed temperature

717   increase over some northern mid-latitude regions between the 20th century and

718   the Little Ice Age based on the CESM-LME, The Holocene, 32, 1251–1259,

719   https://doi.org/10.1177/09596836211041734, 2022.

720 Middleton, N. J. and Thomas, D. S. G.: World atlas of desertification, 2nd edn,

721   Edward Arnold, London, The United Kingdom, 1997.

722 Mishra, V. and Aadhar, S.: Famines and likelihood of consecutive megadroughts in

723   India, npj Clim. Atmos. Sci., 4, 59, https://doi.org/10.1038/s41612-021-00219-1,

724   2021.

725 Monteith, J. L.: Evaporation and environment, Symposia of the Society for

726   Experimental Biology, 19, 205–234, 1965.

727 Ning, L., Chen, K., Liu, J., Liu, Z., Yan, M., Sun, W., Jin, C., and Shi, Z.: How do

728   volcanic eruptions influence decadal megadroughts over eastern China?, J.

729   Climate, 33, 8195–8207, https://doi.org/10.1175/JCLI-D-19-0394.1, 2020.

730 Otto-Bliesner, B. L., Brady, E. C., Fasullo, J., Jahn, A., Landrum, L., Stevenson, S.,

731   Rosenbloom, N., Mai, A., and Strand, G.: Climate variability and change since

732   850 CE: An ensemble approach with the Community Earth System Model, B.

733   Am. Meteorol. Soc., 97, 735–754, https://doi.org/10.1175/bams-d-14-00233.1,

734   2016.

735 PAGES2k Consortium: A global multiproxy database for temperature reconstructions

736   of the Common Era, Sci. Data, 4, 170088, https://doi.org/10.1038/sdata.2017.88,

737   2017.

738 Penman, H. L.: Natural evaporation from open water, bare soil and grass, Proc. R. Soc.

739   Lond. A, 193, 120–145, https://doi.org/10.1098/rspa.1948.0037, 1948.

740 Power, S., Casey, T., Folland, C., Colman, A., and Mehta, V.: Inter-decadal

741   modulation of the impact of ENSO on Australia, Clim. Dynam., 15, 319–324,

742   https://doi.org/10.1007/s003820050284, 1999.

743 Qin, M., Dai, A., Li, D., and Hua, W.: Understanding the inter-decadal variability of

744   autumn precipitation over North Central China using model simulations, Int. J.

745   Climatol., 40, 874–886, https://doi.org/10.1002/joc.6245, 2020.

746 Qin, M., Li, D., Dai, A., Hua, W., and Ma, H.: The influence of the Pacific Decadal

747   Oscillation on North Central China precipitation during boreal autumn, Int. J.

748   Climatol., 38, e821–e831, https://doi.org/10.1002/joc.5410, 2018.

749 Shi, J., Yan, Q., Jiang, D., Min, J., and Jiang, Y.: Precipitation variation over eastern

750   China and arid central Asia during the past millennium and its possible

751   mechanism: Perspectives from PMIP3 experiments, J. Geophys. Res.-Atmos.,

752   121, 11,989–12,004, https://doi.org/10.1002/2016JD025126, 2016.

753 Shi, J., Yan, Q., and Wang, H.: Timescale dependence of the relationship between the

754   East Asian summer monsoon strength and precipitation over eastern China in the

755   last millennium, Clim. Past, 14, 577–591,

756   https://doi.org/10.5194/cp-14-577-2018, 2018.

757 Shi, Y., Shen, Y., Kang, E., Li, D., Ding, Y., Zhang, G., and Hu, R.: Recent and Future

758   climate change in Northwest China, Climatic Change, 80, 379–393,

759   https://doi.org/10.1007/s10584-006-9121-7, 2007.

760 Tardif, R., Hakim, G. J., Perkins, W. A., Horlick, K. A., Erb, M. P., Emile-Geay, J.,

761   Anderson, D. M., Steig, E. J., and Noone, D.: Last Millennium Reanalysis with

762   an expanded proxy database and seasonal proxy modeling, Clim. Past, 15, 1251–

763   1273, https://doi.org/10.5194/cp-15-1251-2019, 2019.

764 Turner, A. G. and Annamalai, H.: Climate change and the South Asian summer

765   monsoon, Nat. Clim. Change, 2, 587–595, https://doi.org/10.1038/nclimate1495,

766   2012.

767 Wang, H. J.: The weakening of the Asian monsoon circulation after the end of 1970's,

768   Adv. Atmos. Sci., 18, 376–386, https://doi.org/10.1007/BF02919316, 2001.

769 Wang, T. and Miao, J. P.: Twentieth-century Pacific Decadal Oscillation simulated by

770   CMIP5 coupled models, Atmos. Ocean Sci. Lett., 11, 94–101,

771   https://doi.org/10.1080/16742834.2017.1381548, 2018.

772   Wang, T., Wang, H. J., Otterå, O. H., Gao, Y. Q., Suo, L. L., Furevik, T., and Yu, L.:

773   Anthropogenic agent implicated as a prime driver of shift in precipitation in

774   eastern China in the late 1970s, Atmos. Chem. Phys., 13, 12433–12450,

775   https://doi.org/10.5194/acp-13-12433-2013, 2013.

776   Wang, T., Xu, H., Jiang, D., and Yao, J.: Mechanisms of reduced mid-Holocene

777   precipitation in arid Central Asia as simulated by PMIP3/4 models, J. Geophys.

778   Res.-Atmos., 127, e2021JD036153, https://doi.org/10.1029/2021JD036153,

779   2022.

780   Webster, P. J. and Yang, S.: Monsoon and ENSO: Selectively interactive systems, Q. J.

781   Roy. Meteor. Soc., 118, 877–926, https://doi.org/10.1002/qj.49711850705, 1992.

782   Xu, H., Wang, T., Wang, H., Chen, S., and Chen, J.: External forcings caused the

783   tripole trend of Asian precipitation during the Holocene, J. Geophys.

784   Res.-Atmos., 128, e2023JD039460, https://doi.org/10.1029/2023JD039460,

785   2023.

786   Xu, H., Wang, T., Wang, H., Miao, J., Chen, J., and Chen, S.: The PMIP3 simulated

787   climate changes over arid Central Asia during the mid-Holocene and last glacial

788   maximum, Acta Geol. Sin.-Engl., 94, 725–742,

789   https://doi.org/10.1111/1755-6724.14542, 2020.

790   Xue, J., Ning, L., Liu, Z., Qin, Y., Chen, K., Yan, M., Liu, J., Wang, L., and Li, C.:

791   The combined influences of solar radiation and PDO on precipitation over

792   eastern China during the last millennium, Clim. Dynam., 60, 1137–1150,

793   https://doi.org/10.1007/s00382-022-06372-4, 2023.

794   Zhang, Y. and Huang, D.: Has the East Asian westerly jet experienced a poleward

795   displacement in recent decades?, Adv. Atmos. Sci., 28, 1259–1265,

796   https://doi.org/10.1007/s00376-011-9185-9, 2011.

797   Zhao, P., Yang, S., and Yu, R.: Long-term changes in rainfall over eastern China and

798   large-scale atmospheric circulation associated with recent global warming, J.

799   Climate, 23, 1544–1562, https://doi.org/10.1175/2009jcli2660.1, 2010.

800   Zhao, X., Dong, B., and Lu, R.: Interdecadal weakening of the cross-equatorial flows

801   over the Maritime Continent during the boreal summer in the mid-1990s: drivers

802   and physical processes, Clim. Dynam., 57, 55–72,

803   https://doi.org/10.1007/s00382-021-05692-1, 2021.

804   Zhu, J., Zhao, K., Wang, Y., Cui, Y., Liang, Y., Cheng, H., Edwards, R. L., Kong, X.,

805   Shao, X., Chen, S., and Pang, L.: Decadal modulation of East Asian summer

806   monsoon variations by external forcing and internal variability, Quaternary Sci.

807   Rev., 293, 107720, https://doi.org/10.1016/j.quascirev.2022.107720, 2022.

808   Zhu, Y., Wang, H., Ma, J., Wang, T., and Sun, J.: Contribution of the phase transition

809   of Pacific Decadal Oscillation to the late 1990s' shift in East China summer

810   rainfall, J. Geophys. Res.-Atmos., 120, 8817–8827,

811   https://doi.org/10.1002/2015JD023545, 2015.